Temporal mixture analysis for estimating impervious surface area from multi-temporal MODIS NDVI data in Japan

doi: 10.1016/j.isprsjprs.2012.05.016

Temporal Mixture Analysis for Estimating Impervious Surface Area from Multi-temporal MODIS NDVI Data in Japan

Fan Yang, Bunkei Matsushita*, Takehiko Fukushima, Wei Yang

Graduate School of Life and Environmental Science, University of Tsukuba

1-1-1, Tennoudai, Tsukuba, Ibaraki. 305-8572, Japan

* Corresponding Author

Tel: +81-29-853-7190

Fax: +81-29-853-7190

E-mail: mbunkei@sakura.cc.tsukuba.ac.jp

Temporal Mixture Analysis for Estimating Impervious Surface Area from Multi-temporal MODIS NDVI Data in Japan

Abstract

As a proxy measure of the human ecological footprint, impervious surface area (ISA) has recently become a key concept in the field of urban remote sensing, with a focus on estimation of the ISA at a city-scale by using Landsat-style satellite images. However, ISA estimation is also in demand in disciplines such as the environmental assessment and policy making at a national scale. This paper proposes a new method for estimating the ISA fraction in Japan based on a temporal mixture analysis (TMA) technique. The required inputs for the proposed method are rearranged MODIS NDVI time-series datasets at the temporal stable zone (i.e., the first to the sixth largest NDVI values in a year). Three ISA distribution maps obtained from Landsat-5 TM data were used as reference maps to evaluate the performance of the proposed method. The results showed that the proposed TMA-based method achieved a large reduction in the effects of endmember variability compared with the previous methods (e.g., SMA and NSMA), and thus the new method has promising accuracy for estimating ISA in Japan. The overall root mean square error (RMSE) of the proposed method was 8.7%, with a coefficient of determination of 0.86, and there was no obvious underestimation or overestimation for the whole ISA range.

Keywords

Impervious surface area, temporal mixture analysis, MODIS, NDVI time-series

1. Introduction

Over the last century, along with the general increase in the rate of human activities, urbanization has become a global trend (Irwin and Bockstael, 2007). Impact from the urbanization process is an important component of urban ecology and is critical not only to the environmental sciences but also for urban engineering (Kaye et al., 2006). Impervious surface area (ISA), which is defined as the area of the constructed surfaces (i.e., roofs, roads, parking lots, and other man-made surfaces) that prevent water from infiltrating into the soil, has been proposed as a useful index to quantify the urbanization process (Arnold and Gibbons, 1996; Sutton et al., 2009).

In the 1970s and 1980s, ISA estimation was carried out mainly using aerial photography (Slonecker et al., 2001). Beginning in the 2000s, in conjunction with the rapid advances in computing power and unmixing techniques, a growing number of studies have employed remote sensing to estimate ISA from satellite sensors (Weng, 2012). However, most of these previous studies have focused on the use of medium spatial resolution images (10-100 m, e.g., Landsat/TM/ETM+, ASTER) at a city- or basin-scale (Ridd 1995; Wu and Murray, 2003; Wu 2004; Lu and Weng, 2006a; Powell et al., 2007; Yang et al., 2010). ISA estimations on a regional, continental, or global scale are still few (Elvidge et al., 2007; Xian and Homer, 2010; Knight and Voth, 2011). This is mainly because the use of medium spatial resolution images for large study areas requires a large number of images and thus is expensive and time-consuming. The use of coarse spatial resolution images such as AVHRR and MODIS (250-1000m) may solve this problem, even though mixed pixels will dominate in these images.

Spectral mixture analysis (SMA) is an approach for decomposing the signal measured at a given pixel into its component parts (i.e., endmembers), and has been widely used in remote sensing of ISA with medium resolution imagery (Weng, 2012). SMA was originally proposed by Adams et al. (1986) and has been improved in recent years (Phinn et al., 2002; Wu and Murray, 2003; Wu 2004; Lu and Weng, 2006b; Powell et al., 2007; Yang et al., 2010). Theoretically, the SMA can be applied to any spatial resolution images provided that the reflectance spectra of endmembers can be obtained. However, the effect of the spectral complexity within endmembers on the accuracy of ISA estimation remains a major problem,

especially when using a coarse spatial resolution image over a large area (Matsushita and Fukushima, 2009; Yang et al., 2010; Somers et al., 2011).

However, because the coarse spatial resolution sensors all have higher temporal resolution (about 1 day), it may be possible to use another mixture analysis technique, that is, temporal mixture analysis (TMA), to estimate ISA based on the temporal characteristics of the land cover types. The TMA, which is algebraically identical to the SMA but uses temporal spectra instead of electromagnetic spectra, was first proposed by Piwowar et al. (1998), and has been mainly applied in the agriculture field of remote sensing (Defries et al., 2000; Lobell and Asner, 2004). As has been suggested previously, the TMA has good potential for use in reducing endmember variability and thus could provide an improved ISA estimation (Somers et al., 2011).

Consequently, the objectives of this study were: (1) to develop a new TMA-based method that can accurately estimate ISA at a large scale in Japan as a case study, and (2) to evaluate the performance of the proposed method by comparing it with several previous methods (e.g., SMA-based methods and regression analysis method).

2. Materials

MODIS NDVI time-series datasets (MOD13Q1) for 2001 and 2007 were downloaded from the NASA website through the Warehouse Inventory Search Tool (WIST). These datasets had a spatial resolution of 250 m and were 16-day composited using the BRDF method. This composite MODIS product contains six layers: they are NDVI, EVI, and reflectance at blue, red, near infrared and middle infrared bands. The area of Japan was then subset from the global dataset, and the extracted NDVI temporal profile was further smoothed using a Savitzky-Golay filter (Savitzky and Golay 1964)-based method to reduce the remaining cloud/noise effects in the NDVI time-series datasets (Chen et al., 2004).

A vegetation map obtained from the fifth survey of the green census by the Natural Conservation Bureau of the Ministry of the Environment of Japan was utilized to extract vegetation pixels from NDVI time-series datasets. The original vegetation map is archived in vector format and contains 58 main vegetation types (Matsushita et al., 2006). According to the purpose of this study, the vegetation map was

merged into 12 new classes, namely alpine scrub/snow patch, subalpine needle leaf forest, deciduous needle leaf forest, evergreen needle leaf forest, deciduous broadleaf forest, evergreen broadleaf forest, wetland, orchard, grassland, bamboo, crop field and urban area. Then this new vegetation map was converted from vector to raster format (using the area prior method) at 250 m spatial resolution to correspond with the NDVI time-series datasets (Fig. 1).

(Please insert Fig. 1 here)

It can be considered that the vegetation pixels in the above vegetation map contained many mixed pixels (i.e., pixels including vegetation and non-vegetation) due to the coarse spatial resolution (250 m, with geographic error around 5 m). To further extract pure vegetation pixels, another dataset, road and building map (vector format) provided by Geospatial Information Authority of Japan (GSI), was employed. This road and building map was also converted from vector to raster format at 250 m spatial resolution (the pixels with roads, buildings or both were recorded as 1, and the others were recorded as 0). By combining vegetation as well as road and building maps, vegetation pixels without any road and building information were extracted as pure vegetation pixels and other pixels were masked out. This new vegetation map was designated a pure vegetation map.

Three Landsat-5 TM Images covering Sapporo City (in Hokkaido Prefecture) in Northern Japan on July 31, 2007, Kanto Plain in Eastern Japan on July 11, 2000 and Kagoshima City (in Kagoshima Prefecture) in Southern Japan (Fig.1) on February 13, 2000, were used to generate the ISA reference map for accuracy assessment. The Landsat-5 TM Image-based ISA fractions were estimated using the pre-screened and normalized multiple endmember spectral mixture analysis (PNMESMA) method (Yang et al, 2010). In the PNMESMA, exclusion of pure vegetation pixels in advance and NSMA and MESMA approaches are combined to improve the accuracy of ISA estimation. Validation by using aerial photographs (with 0.5m spatial resolution) showed that the estimation error (overall RMSE) of PNMESMA was 5.2%, and no obvious underestimation or overestimation occurred for high or low imperious surface areas (Yang et al., 2010). The Landsat-5 TM Image-based ISA fraction maps were then re-sampled (pixel aggregated) to 250 m to correspond with the spatial resolution of the MODIS data.

3. Methods

3.1 Temporal mixture analysis of NDVI profile

The temporal NDVI profile has been widely used for estimation of the vegetation fraction (Defries et al., 2000; Lobell and Asner, 2004; Xiao and Moody, 2005; Ozdogan, M., 2010). Temporal mixture analysis is based on the empirical fraction-NDVI relationship, in which the NDVI value of a mixed pixel is the linear combination of NDVI values of endmembers (Wittich and Hansing, 1995; Xiao and Moody, 2005). Mathematically, this relation can be written as:

$$NDVI_{mix} = \sum_{i=1}^{N} f_i NDVI_i + \varepsilon \quad (1)$$

where $NDVI_{mix}$ is the temporal profile of NDVI of the target pixel; $NDVI_i$ is the temporal NDVI signature of the endmember i; f_i is the fraction of the endmember i, and ε is the residual representing model error. The fractions of the endmembers are commonly constrained by

$$\sum_{i=1}^{N} f_i = 1, \ f_i \geq 0 \quad (2)$$

The fraction of each endmember can be obtained using the least-squares method.

3.2 Temporal characteristics of major vegetation types in Japan

Based on the pure vegetation map and smoothed NDVI time-series datasets, the temporal profiles of major vegetation types in Japan were investigated to capture their phenological characteristics. As an example, Fig. 2a shows several NDVI temporal profiles for each of four major forests (i.e., an evergreen needleleaf forest, a deciduous needleleaf forest, an evergreen broadleaf forest and a deciduous broadleaf forest) located in different areas of Japan. It can be seen that the evergreen and deciduous forests present very different NDVI temporal profiles due to their different physiological properties. Even among the three different deciduous (and three different evergreen) forests, the NDVI temporal profiles are different (e.g., green-up periods differ) because of the different climates in different regions of Japan. This problem did not become prominent in previous studies that focused on certain small farm areas (Oleson et al., 1995; Lobell and Asner, 2004; Ozdogan, 2010; Verbesselt et al., 2010; De Jong et al., 2011). The NDVI temporal profiles for crop vegetation (another major vegetation type in Japan, accounting for 16.5% of

total surface area), which showed longer green-up periods and shorter maximum NDVI periods, are very different from those for forests (Fig. 2b). Therefore, it is difficult to use one NDVI temporal profile of vegetation to represent the vegetation endmember in TMA. The larger endmember variability will result in noticeable errors in ISA estimation on a large scale (e.g., on a national scale). However, it should be noted that if these NDVI temporal profiles could be shifted along the time axis the variability within endmembers would be reduced, especially at larger NDVI values.

In consideration of the above, the NDVI temporal profiles shown in Fig. 2a and b were rearranged from minimum to maximum according to the values of NDVI (Fig. 2c and d). It can be seen that the NDVI temporal profiles were similar in the high NDVI value zone while they showed large variation in the low NDVI value zone. The reason for the variation in the low NDVI zone of the same vegetation class was probably related to the different covering conditions in winter (presence/absence of snow cover, different methods of land maintenance for farmland and so on). To further demonstrate the temporal characteristics of vegetation in Japan, the NDVI temporal profiles of all extracted pure vegetation pixels were rearranged and averaged for each vegetation type, and the standard deviation for each period was also calculated (Fig. 3). The results show that all forest types have similar NDVI temporal profiles in the high NDVI value zone, especially for the last six maximum NDVI values. However, in the low NDVI zone, their NDVI temporal profiles are very different. The NDVI temporal profiles of crop vegetation are different from those of forest vegetation; the former show a rapidly increasing trend compared with forest vegetation types even in the high NDVI zone. The standard deviations in the high NDVI zone are significantly smaller than those in the low NDVI zone for all vegetation types. This indicates that the variation of NDVI temporal profile in the high NDVI value zone is smaller than that in the low NDVI value zone for each vegetation type, and thus the NDVI temporal profile in the high NDVI zone has the potential to be summarized as an endmember.

(Please insert Fig.2 here)

(Please insert Fig.3 here)

3.3 Development of a new TMA-based method for estimating ISA in Japan

Based on the results of the preparatory investigation above, a new TMA-based method was proposed for estimating the ISA fraction from NDVI time-series datasets.

First, MODIS NDVI time-series datasets (MOD13Q1) for 2001 were rearranged according to the values of NDVI, and the last six maximum NDVI time-series datasets for Japan were then extracted. Second, principal component analysis (PCA) was carried out for the extracted NDVI time-series datasets to guide endmember selection for TMA (Smith et al., 1985). It can be seen that the first and second principal components (PCs) represented 99.8% of the variances contained in the extracted NDVI time-series datasets. From the feature space representation of the first two PC components, three endmembers (i.e., pixels distributing on the apex of a triangle) can be identified (Fig.4). They are forest, crop and ISA. The averaged NDVI temporal profiles of the selected three endmembers with their standard deviation and relative standard deviation are shown in Table 1a. Finally, for a given pixel, by using the linear mixture model of TMA (Eq. 1) with the selected three endmembers, the fraction of each endmember can be calculated.

(Please insert Fig.4 here)

(Please insert Table 1 here)

3.4 Accuracy assessment

A 3 × 3 sampling unit (750 m × 750 m) was utilized to reduce the impact of geometric errors associated with the MODIS and Landsat-5 TM images. Each ISA reference map (re-sampled Landsat-5 TM Image-based ISA fraction map) was equally segmented into 20×20 meshes, and the pixel located in the center of each mesh along with its eight neighboring pixels (i.e., for a 3 × 3 sampling unit= 750 m × 750 m) was extracted for accuracy assessment. In addition, sampling units that contained water- or cloud-contaminated pixels were excluded from the accuracy assessment procedure. Therefore, there were 135, 281 and 133 sampling units left in Kagoshima, Kanto Plain and Sapporo, respectively, to assess the ISA estimation accuracy for different methods.

The error was quantified by the root mean square error (RMSE) as well as the mean bias (MB), and these terms were defined as follows:

$$RMSE = \sqrt{\sum_{i=1}^{N} (ISA_{modis,i} - ISA_{landsat,i})^2 / N} \quad (3)$$

$$MB = \sum_{i=1}^{N} (ISA_{modis,i} - ISA_{landsat,i}) / N \quad (4)$$

where $ISA_{modis,i}$ is the ISA fraction estimated from MODIS data, and $ISA_{landsat,i}$ is the ISA fraction estimated from Landsat-5 TM data for the sampling unit i, respectively. N is the number of the sampling units for validation (total 547 in this study).

4. Results

4.1 Performance of the proposed TMA-based method

The ISA fraction map estimated by using the proposed method is shown in Fig.5. It can be seen that the high ISA fraction was mainly distributed in several large cities, such as Sapporo, Tokyo, Nagoya and Osaka; the middle ISA fraction was found in other cities and rural areas; and the low ISA fraction was almost completely distributed in the forest area, which is the largest land cover type in Japan.

(Please insert Fig.5)

The ISA-fraction distribution maps obtained from Landsat-5 TM images based on the PNMESMA method and from MODIS NDVI time-series datasets based on the proposed TMA-based method are shown in Fig. 6 for visual comparison. It can be seen that there is a similar distribution pattern between two ISA maps for all three testing sites, despite the fact that they were obtained from different satellite sensors based on different methods. These results indicate that the proposed TMA-based method has good potential for use in conjunction with the MODIS sensor to provide ISA estimation with accuracy similar to that of the Landsat-5 TM sensor, even though these two sensors have very different spatial resolutions (250 m vs. 30 m).

The ISA estimated from MODIS NDVI-time-series datasets using the proposed TMA-based method was also quantitatively compared with that estimated from Landsat-5 TM images based on PNMESMA method. The results are shown in Fig. 7a. The overall RMSE of the proposed TMA-based method is 0.087, and with slightly underestimation (MB=-0.014). The coefficient of determination is 0.86, which indicates

that 86% of the variance in the ISA estimations from MODIS NDVI time-series datasets correspond with those from Landsat-5 TM spectral reflectance data.

(Please insert Fig.6 here)

(Please insert Fig.7 here)

4.2 Comparison with other methods

The ISA estimated from MODIS spectral reflectance data based on the previous SMA and NSMA methods as well as a global ISA map produced by Elvidge et al. (2007) were compared with the ISA estimated by the proposed TMA-based method described in Section 3.3 (see the Appendix for descriptions of the three previous methods). For the SMA and NSMA methods, the same pure pixels obtained from Fig. 4 (i.e., forest, crop and ISA) were used to generate the endmembers, but with reflectance spectra instead of an NDVI temporal profile. To further reduce cloud contamination and bare soil effects in the datasets, these time-series images were composited as one image using the maximum NDVI method. The corresponding reflectance spectra at four bands in the final composited image in 2001 (for Kanto and Kagoshima) and 2007 (for Sapporo) were used to test the SMA and NSMA methods. The endmembers as well as the standard deviation (SD) and relative standard deviation (RSD) for the SMA and NSMA methods are shown in Table 1b and 1c.

The results of the accuracy assessment for the previous methods are also shown in Fig.7. The results shown in Fig. 7b indicate that the SMA method has large estimation error and the overestimations with RMSE and MB were 0.159 and 0.038, respectively. The results shown in Fig. 7c suggest that the NSMA method improved the ISA estimation accuracy compared with the SMA method (RMSE=0.126 with MB=0.021), especially in low ISA areas. The Global ISA map shows large underestimation in the low ISA areas and a large overestimation in the high ISA areas, with the largest overall RMSE of 0.176 and MB of -0.045 for all samples. This result indicated that the regression model constructed using the data only from America is not suitable to estimate the ISA in Japan, probably because of the different patterns in population distribution and nighttime light usage between Japan and America.

Compared with the previous methods, the TMA gave the best performance among the four methods. The determination coefficients of the three previous methods were 0.63 (the SMA method), 0.80 (the NSMA method), and 0.51 (the global ISA map), respectively, which also were lower than that of the proposed TMA-based method, indicating that the variances in the ISA estimations from MODIS spectral reflectance data based on the SMA or NSMA method, as well as the global ISA map, were smaller than the corresponding values from the Landsat-5 TM spectral reflectance data.

5. Discussion

The variability within an endmember class due to spectral complexity of many land cover types is the most profound source of error in ISA estimation (Yang et al., 2010; Somers et al., 2011). Therefore, how to address endmember variability is a key for accurate ISA estimation. Although many techniques have been proposed to reduce the errors related to endmember variability, it is still a challenge to completely remove the brightness variation within an endmember (Somers et al., 2011). The TMA using temporal features instead of spectral features in SMA or NSMA provides an alternative to further reduce endmember variability. From table 1, it can be seen that even when the same pixels were selected to generate endmembers for TMA, SMA, and NSMA, the endmembers in the TMA gave the smallest variation (RSD less than 9%, 1.7%, and 5.1% for ISA, forest, and crop, respectively) while the endmembers in the SMA showed the largest variation (RSD between 59.3-78.2%, 28.1-113.2%, and 18.5-59.1% for ISA, forest, and crop, respectively). Although the NSMA was proposed to reduce the endmember variability in SMA, a large variation in NSMA endmembers remained (RSD between 51.7-65.9%, 6.5-109.7%, and 10.3-55.7% for ISA, forest, and crop, respectively). This is because the use of rearranged NDVI time-series datasets in a stable temporal zone (i.e., the last six maximum NDVI) can not only reduce the effects due to shade and topography (Matsushita et al., 2007), but also the effects due to different vegetation phenologies under different meteorological condition. Therefore, the proposed TMA-based method has a promising level of accuracy for estimating ISA in Japan.

It can be considered that implementing the MESMA technique into TMA may further reduce endmember variability, and thus promise more accurate ISA estimation. However, the results obtained

from a simple MESMA-technique-integrated method (three endmembers for forest, crop, and ISA, respectively; i.e., the maximum, minimum and mean values of selected endmembers from Fig. 4) do not show any improvement compared with the use of only one standardized temporal profile for each endmember (slightly decreased R^2 of 0.841 and slightly increased RMSE of 0.091). This result indicates that selecting endmembers from rearranged NDVI time-series datasets in a stable temporal zone may sufficiently reduce endmember variability, and thus can overcome the major drawback (computational complexity) of the MESMA technique. In addition, successful use of MESMA technique is highly dependent on a comprehensive endmember library, which is difficult to obtain from a practical standpoint.

Another advantage of the proposed TMA-based method is that it provides an opportunity to separate the vegetation endmembers into two types: forests or crops. In addition to the ISA, the crop is also an important proxy measure of the human ecological footprint. However, since the spectral features between crops and forests are very similar, both land cover types are often concentrated at the same locations in the feature space representations and then identified as one vegetation endmember in SMA and NSMA. In contrast, Nemani and Running (1997) reported that the phenological evolutions of crops are different from those of forests; generally, forests achieve maximum canopy covers within a few weeks whereas crops take longer time to achieve full canopy cover. This phenomenon can also be seen from Fig. 3. Therefore, by using temporal features in TMA instead of spectral features in SMA and NSMA, separation of forests and crops becomes possible (Fig. 4). Further studies will be needed to explore this possibility.

Furthermore, other satellite sensors, such as NOAA/AVHRR and SPOT/Vegetation, can also provide the NDVI time-series datasets. These datasets not only allow long-term data accumulation at a global scale, but are also available without cost. Therefore, these advantages of the TMA-based method would allow investigation of the global distribution and long-term changes of ISA, and thereby the ways in which human beings have modified the environment of Earth.

In this study, the effects of bare soil were not considered because bare soil is not a major land cover type in Japan. However, for applying the proposed TMA-based method to areas that include a lot of bare soils or deserts, these effects could be substantial, because bare soil and sand have NDVI temporal profiles similar to those of the ISA. In these cases, ancillary data obtained from DMSP/OLS have the potential to

remove the effects of soils (Elvidge et al., 2007). In addition, the TMA cannot be applied to satellite data with high spatial resolution, because this kind of satellite data always shows low temporal resolution, and thus it would not provide appropriate temporal profiles for the TMA.

Another important issue is the use of linear combinations of NDVI in the mixture model. Although the nonlinear characteristics of NDVI combinations have been discussed in previous studies (Carlson and Ripley, 1997; Lobell and Asner, 2004), an empirical linear model was widely applied because it is simple but efficient for computation (Wittich and Hansing, 1995; Gutman and Ignatov, 1998; Xiao and Moody, 2005; Knight and Voth, 2011). Song (2005) discussed this problem and found that NDVI could be linearly related to the vegetation fraction when the background was brighter, and thus it is reasonable to apply a linear unmixing model for NDVI in urban environments. In addition, Xiao and Moody (2005) also found that the response of NDVI to the vegetation fraction could be linear in similar ecosystems and at similar phenological stages. The rearrangement of the NDVI time-series in this study can normalize the phenological stages and thus strengthened the above empirical conditions. The results of this study also showed that the linear unmixing of NDVI is feasible to estimate the fraction of the impervious surface for our study area. Further studies will be needed to explore the performance of the proposed TMA-based method in other areas.

6. Conclusions

A new method based on TMA was proposed to estimate the ISA fraction in Japan. The required inputs for the proposed method are rearranged NDVI time-series datasets at the temporal stable zone (i.e., the last six maximum NDVI values in a year). Compared with the previous ISA estimation methods, the proposed TMA-based method resulted in a significant reduction in the effects of endmember variability, and thus provided a result corresponding with 86% variance in the ISA estimations from Landsat-5 TM spectral reflectance data. The overall RMSE was also reduced from 0.176 (global ISA map), 0.159 (SMA) or 0.126 (NSMA) to 0.087, and there was no obvious underestimation or overestimation for the whole ISA range.

Appendix. Three previous methods for estimating the impervious surface area

The first method for comparison is the SMA. For a given pixel, the reflectance for each band b (R_b) can be written as:

$$R_b = \sum_{i=1}^{N} f_i R_{i,b} + e_b \quad \text{(A-1)}$$

$$\sum_{i=1}^{N} f_i = 1, \; f_i \geq 0 \quad \text{(A-2)}$$

where N is the number of endmembers (i.e., spectrally "pure" materials), f_j is the fraction of endmember j, $R_{j,b}$ is the reflectance of endmember j in band b, and e_b is the unmodeled residual indicating the disagreement between the measured and modeled spectra in band b. The fraction of each endmember can be obtained using the least-squares method.

The second method is the NSMA method (Wu, 2004). In the NSMA, the normalized reflectance spectra of each pixel and endmember were used instead of the reflectance spectra in the SMA model. The normalized reflectance for band b in a pixel ($\overline{R_b}$) can be written as:

$$\overline{R_b} = R_b / \mu \quad \text{(A-3)}$$

$$\mu = \sum_{b=1}^{M} R_b / M \quad \text{(A-4)}$$

where μ is the average reflectance for all bands of that pixel, M is the total number of bands, and R_b is the reflectance for band b.

The third method is based on a multiple linear regression model using the nighttime light and population as independent variables, which is written as (Elvidge et al., 2007):

Percent cover of ISA = 0.00795 (radiance) + 0.00868 (population count) (A-5)

where radiance is estimated from calibrated nighttime lights of the U.S. Air Force Defense Meteorological Satellite Program (DMSP) Operational Linescan System (OLS), and the population count is obtained from Landscan 2004 made by the U.S. Department of Energy, Oak Ridge National Laboratory. In this study, the global ISA map of 2000-2001 based on Equation (A-5) was directly downloaded from DMSP products in the National Oceanic and Atmospheric Administration (NOAA). Since the global ISA map in 2007 is not

available, only the Landsat-5 TM images of Kanto Plain and Kagoshima (totally 414 sampling units) were used to assess the accuracy.

Acknowledge

This study was supported by the Environment Research and Technology Development Fund (S-9-4-(1)) of the Ministry of the Environment, Japan and Grants-in-Aid for Scientific Research of MEXT from Japan (No. 21401001). The valuable comments from reviewers improved the scientific level of this paper. The authors are thankful to Dr. Ishitsuka N. in National Institute for Agro-Environmental Sciences (NIAES) for the discussion during the data processing and paper composing. Special thanks should be given to Ms. Iguchi L. and Mr. Makabe T. for efficient assistant in data pre-processing.

Reference

Adams, J.B., Smith, M.O., Johnson, P.E., 1986. Spectral Mixture Modeling: A New Analysis of Rock and Soil Types at the Viking Lander 1 Site. Journal of Geophysical Research, 91(B8), 8098-8112.

Arnold, C.L., Gibbons, C.J., 1996. Impervious surface coverage: the emergence of a key environmental indicator. Journal of the American Planning Association, 62(2), 243–258.

Carlson, T. N., and Riziley, D. A., 1997. On the relation between NDVI, fractional vegetation cover, and leaf area index. Remote Sensing of Environment, 62(3), 241-252.

Chen, J., Jönsson, P., Tamura, M., Gu, Z., Matsushita, B., Eklundh, L., 2004. A simple method for reconstructing a high-quality NDVI time-series data set based on the Savitzky-Golay filter. Remote Sensing of Environment, 91(3-4), 332-344.

De Jong, R., Bruin, S., Wit, A., Schaepman, M. E., Dent, D. L., 2011. Analysis of monotonic greening and browning trends from global NDVI time-series. Remote Sensing of Environment, 115(2), 692-702.

Defense Meteorological Satellite Program (DMSP) products in the National Oceanic and Atmospheric Administration (NOAA), http://www.ngdc.noaa.gov/dmsp/ (Accessed 2 September, 2011)

Defries, S., Hansen, M.C., Townshend, J.R.G., 2000. Global continuous fields of vegetation characteristics: a linear mixture model applied to multi-year 8 km AVHRR data. International Journal of Remote Sensing, 21(6-7), 1389-1414.

Elvidge, C.D., Tuttle, B.T., Sutton, P.C., Baugh, K.E., Howard, A.T., Milesi, C., Bhaduri, B., Nemani, R., 2007. Global distribution and density of constructed impervious surfaces. Sensors, 7(9), 1962–1979.

Gutman, G., Ignatov, A., 1998. The derivation of the green vegetation fraction from NOAA_AVHRR data for use in numerical weather prediction models. International Journal of Remote Sensing, 19(8), 1533–1543.

Irwin, E.G., Bockstael, N.E., 2007. The evolution of urban sprawl: evidence of spatial heterogeneity and increasing land fragmentation. Proceedings of the National Academy of Sciences of the United States of America, 104(52), 20672-20677.

Kaye, J.P., Groffman, P.M., Grimm, N.B., Baker, L., Pouyat, R.V., 2006. A distinct urban biogeochemistry? Trends in ecology and evolution, 21(4), 192-199.

Knight, J., Voth, M., 2011. Mapping Impervious Cover Using Multi-Temporal MODIS NDVI Data. IEEE Journal of Selected Topics in Applied Earth Observations and Remote Sensing, 4(2), 303－309.

Lobell, D.B., Asner, G.P., 2004. Cropland distributions from temporal unmixing of MODIS data. Remote Sensing of Environment, 93(3), 412-422.

Lu, D., Weng, Q., 2006a. Spectral mixture analysis of ASTER images for examining the relationship between urban thermal features and biophysical descriptors in Indianapolis, Indiana, USA. Remote Sensing of Environment, 104(2), 157-167.

Lu, D., Weng, Q., 2006b. Use of impervious surface in urban land-use classification. Remote Sensing of Environment, 102(1-2), 146-160.

1 Matsushita, B., Fukushima, T., 2009. Methods for retrieving hydrologically significant surface parameters
2 from remote sensing: a review for applications to east Asia region. Hydrological Processes, 23(4),
3 524- 533.

4 Matsushita, B, Xu, M., Fukushima, T., 2006. Characterizing the changes in landscape structure in the Lake
5 Kasumigaura Basin, Japan using a high-quality GIS dataset. Landscape and Urban Planning, 78(3),
6 241-250.

7 Matsushita, B., Yang, W., Chen, J., Onda, Y., Qiu, G., 2007. Sensitivity of the Enhanced Vegetation Index
8 (EVI) and Normalized Difference Vegetation Index (NDVI) to topographic effects: A case study in
9 high-density cypress forest. Sensors, 7(11), 2636-2651.

10 Nemani, R., Running, S., 1997. Land cover characterization using multitemporal red, near-IR, and
11 thermal-IR data from NOAA/AVHRR. Ecological Applications, *7*(1), 79–90.

12 Oleson, K.W., Sarlin, S., Garrison, J., Smith, S., Privette, J.L., Emery, W.J., 1995. Unmixing multiple
13 land-cover type reflectances from coarse spatial resolution satellite data. Remote Sensing of
14 Environment, 54(2), 98-112.

15 Ozdogan, M., 2010. The spatial distribution of crop types from MODIS data: Temporal unmixing using
16 Independent Component Analysis. Remote Sensing of Environment, 114(6), 1190-1204.

17 Phinn, S., Stanford, M., Scarth, P., Murray, A. T., Shyy, P. T., 2002. Monitoring the composition of urban
18 environments based on the vegetation-impervious surface-soil (VIS) model by subpixel analysis
19 techniques. International Journal of Remote Sensing, 23(20), 4131-4153.

20 Piwowar, J.M., Peddle, D.R., LeDrew, E.F., 1998. Temporal mixture analysis of arctic sea ice imagery: a
21 new approach for monitoring environmental change. Remote sensing of environment, 63(3), 195–
22 207.

23 Powell, R.L., Roberts, D.A., Dennison, P.E., Hess, L.L., 2007. Sub-pixel mapping of urban land cover
24 using multiple endmember spectral mixture analysis: Manaus, Brazil. Remote Sensing of
25 Environment, 106(2), 253-267.

26 Ridd, M.K., 1995. Exploring a V-I-S (vegetation-impervious surface-soil) model for urban ecosystem
27 analysis through remote sensing: comparative anatomy for cities. International Journal of Remote
28 Sensing, 16(12), 2165-2185.

29 Roberts, D., Gardner, M., Church, R., Ustin, S., Scheer, G., Green, R., 1998. Mapping Chaparral in the
30 Santa Monica Mountains Using Multiple Endmember Spectral Mixture Models. Remote Sensing of
31 Environment, 65(3): 267-279.

32 Savitzky, A., Golay, M.J.E., 1964. Smoothing and Differentiation of Data by Simplified Least Squares
33 Procedures. Analytical chemistry, 36(8), 1627–1639.

34 Sloneckera, E.T., Jenningsa, B.D., Garofalo, D., 2001. Remote sensing of impervious surface: a review.
35 Remote Sensing Review, 20(3), 227–235.

36 Smith, M.O., Johnson, P.E., and Adams, J.B., 1985. Quantitative Determination of Mineral Types and
37 Abundances from Reflectance Spectra Using Principal Components Analysis. Journal of
38 Geophysical Research, 90(C), 797-804.

Somers, B., Asner, G. P., Tits, L., Coppin, P., 2011. Endmember variability in Spectral Mixture Analysis: A review. Remote Sensing of Environment, 115(7), 1603-1616.

Song, C., 2005. Spectral mixture analysis for subpixel vegetation fractions in the urban environment: How to incorporate endmember variability? Remote Sensing of Environment, 95(2), 248-263.

Sutton, P.C., Anderson, S.J., Elvidge, C.D., Tuttle, B.T., Ghosh, T., 2009. Paving the planet: impervious surface as proxy measure of the human ecological footprint. Progress in Physical Geography, 33(4), 510-527.

Verbesselt, J., Hyndman, R., Zeileis, A., Culvenor, D., 2010. Phenological change detection while accounting for abrupt and gradual trends in satellite image time series. Remote Sensing of Environment, 114(12), 2970-2980.

Weng, Q., 2012. Remote sensing of impervious surfaces in the urban areas: Requirements, methods, and trends. Remote Sensing of Environment, 117(2), 34-49.

Wittich, K., Hansing, O., 1995. Area-averaged vegetative cover fraction estimated from satellite data. International Journal of Biometeorology, 38(4), 209-215.

Wu, C., 2004. Normalized spectral mixture analysis for monitoring urban composition using ETM+ imagery. Remote Sensing of Environment, 93(4), 480-492.

Wu, C., Murray, A.T., 2003. Estimating impervious surface distribution by spectral mixture analysis. Remote Sensing of Environment, 84(4), 493-505.

Xian, G., Homer, C., 2010. Updating the 2001 National Land Cover Database Impervious Surface Products to 2006 using Landsat Imagery Change Detection Methods. Remote Sensing of Environment, 114(8), 1676-1686.

Xiao, J., Moody, A., 2005. A comparison of methods for estimating fractional green vegetation cover within a desert-to-upland transition zone in central New Mexico, USA. Remote Sensing of Environment, 98(2-3), 237-250.

Yang, F., Matsushita, B., Fukushima, T., 2010. A pre-screened and normalized multiple endmember spectral mixture analysis for mapping impervious surface area in Lake Kasumigaura Basin, Japan. ISPRS Journal of Photogrammetry and Remote Sensing, 65(5), 479-490.

1 Tables

2 Table 1 Endmembers for each method (a-TMA; b-SMA; c-NSMA, see Appendix for details of SMA and

3 NSMA)

A

Temporal profile	ISA			Forest			Crop		
	Mean	SD	RSD	Mean	SD	RSD	Mean	SD	RSD
No.18	0.166	0.015	9.0%	0.898	0.015	1.7%	0.596	0.020	3.4%
No.19	0.170	0.014	8.4%	0.905	0.015	1.6%	0.667	0.034	5.1%
No.20	0.175	0.014	7.8%	0.912	0.014	1.6%	0.741	0.021	2.8%
No.21	0.180	0.013	7.5%	0.917	0.014	1.6%	0.796	0.023	2.8%
No.22	0.185	0.013	7.1%	0.922	0.015	1.6%	0.849	0.017	1.9%
No.23	0.188	0.013	6.9%	0.926	0.015	1.6%	0.870	0.014	1.6%

4

B

Spectral profile	ISA			Forest			Crop		
	Mean	SD	RSD	Mean	SD	RSD	Mean	SD	RSD
Band 1	0.028	0.021	76.1%	0.008	0.009	113.2%	0.019	0.011	59.1%
Band 2	0.047	0.034	72.6%	0.012	0.006	50.0%	0.032	0.012	36.8%
Band 3	0.095	0.075	78.2%	0.285	0.080	28.1%	0.362	0.067	18.5%
Band 4	0.079	0.047	59.3%	0.046	0.018	39.4%	0.081	0.021	25.9%

5

C

Spectral profile	ISA			Forest			Crop		
	Mean	SD	RSD	Mean	SD	RSD	Mean	SD	RSD
Band 1	0.410	0.271	65.9%	0.090	0.098	109.7%	0.151	0.084	55.7%
Band 2	0.631	0.326	51.7%	0.130	0.045	35.0%	0.258	0.088	34.1%
Band 3	1.276	0.663	52.0%	3.260	0.210	6.5%	2.919	0.299	10.3%
Band 4	1.210	0.645	53.3%	0.518	0.129	24.8%	0.657	0.136	20.7%

6

7 Mean column is the mean value of the temporal/spectral profiles for each endmember (temporal/spectral
8 signature); SD column is the standard deviation of the temporal/spectral profiles for each endmember,
9 which means the inherent variation in the temporal/spectral signature of the endmember). To compare the
10 variations among different methods, the RSD (relative standard deviation, =SD/mean) was also calculated.

Figures

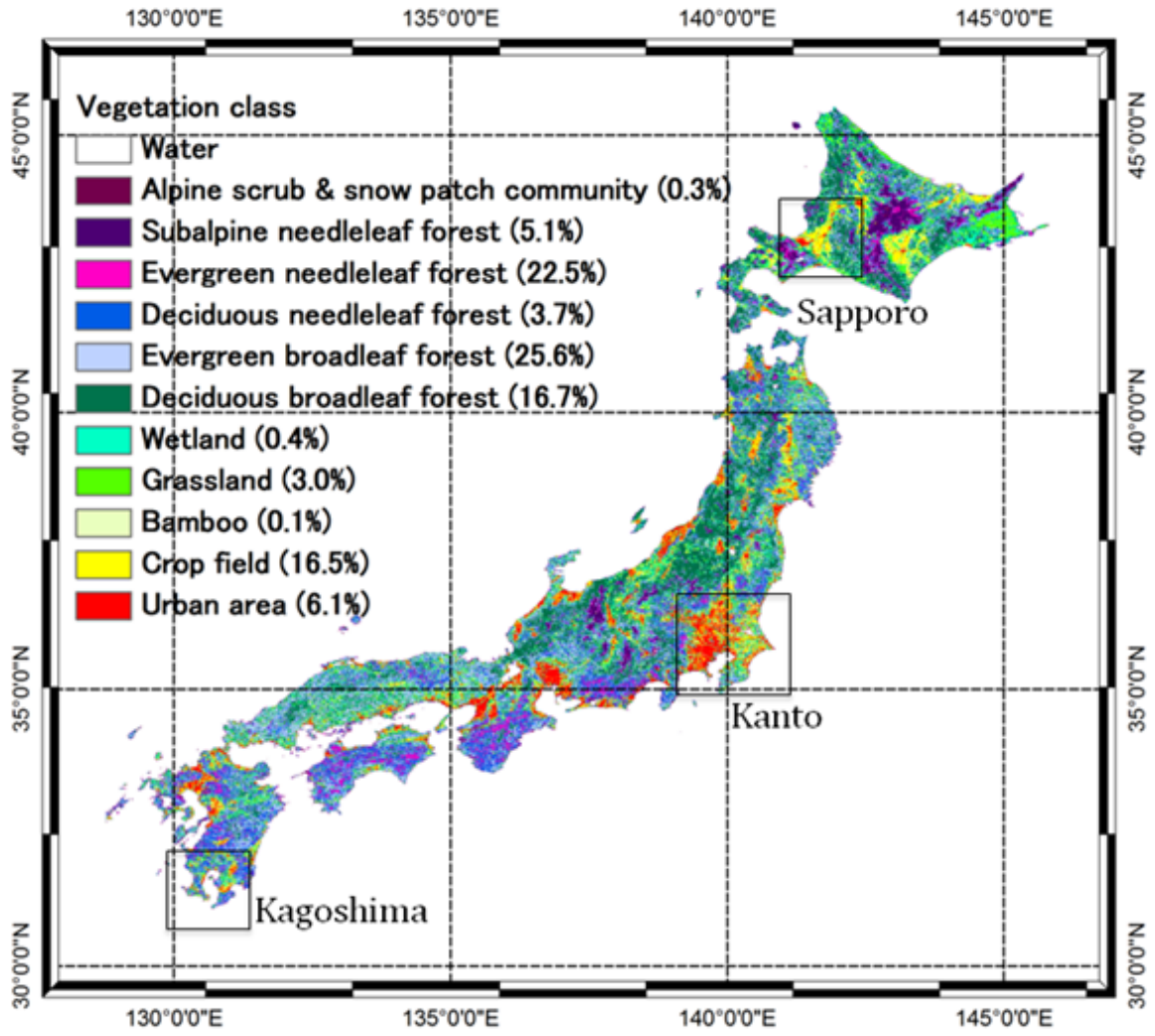

Fig.1 Rasterized actual vegetation map. The actual vegetation vector map according to the 5th survey by Ministry of the Environment (Japan) was re-classified to 12 classes and rasterized (using area prior) to the spatial resolution of 250 m. The coverage of each class was calculated. For the accuracy assessment, Sapporo City in the north, Kanto Plain in the east and Kagoshima City in the south were selected and Landsat images of these three areas were prepared.

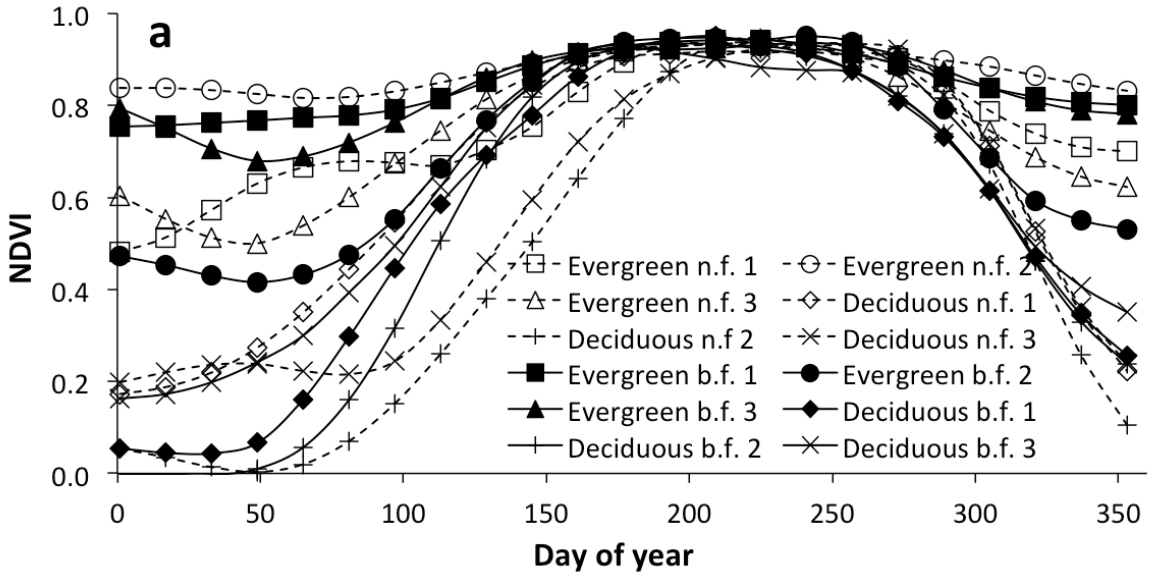
a
NDVI
Day of year
Evergreen n.f. 1
Evergreen n.f. 2
Evergreen n.f. 3
Deciduous n.f. 1
Deciduous n.f 2
Deciduous n.f. 3
Evergreen b.f. 1
Evergreen b.f. 2
Evergreen b.f. 3
Deciduous b.f. 1
Deciduous b.f. 2
Deciduous b.f. 3

1

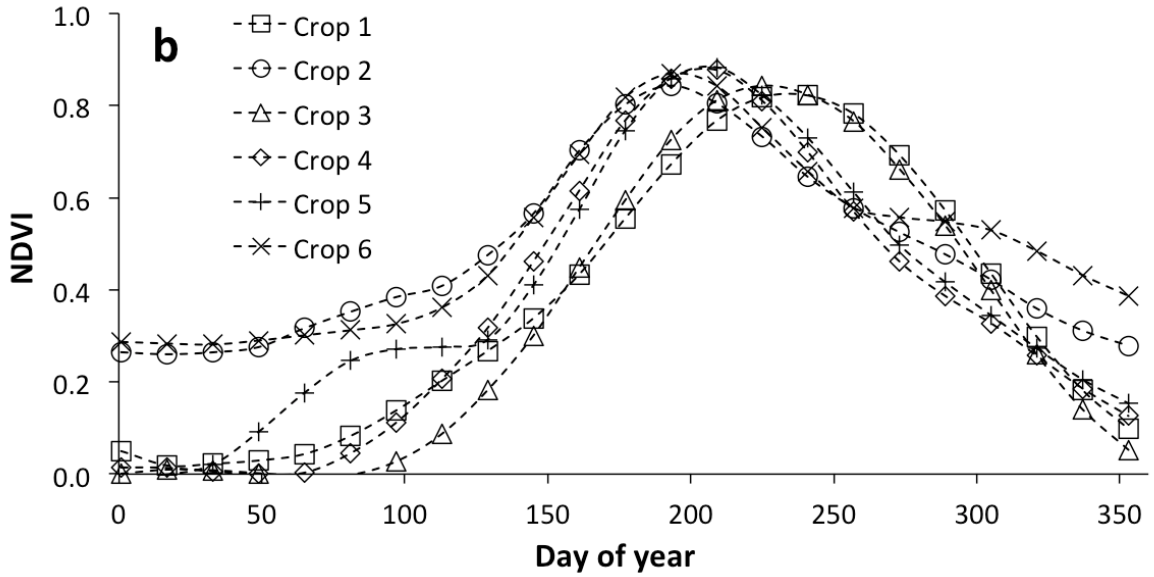
b
NDVI
Day of year
Crop 1
Crop 2
Crop 3
Crop 4
Crop 5
Crop 6

2

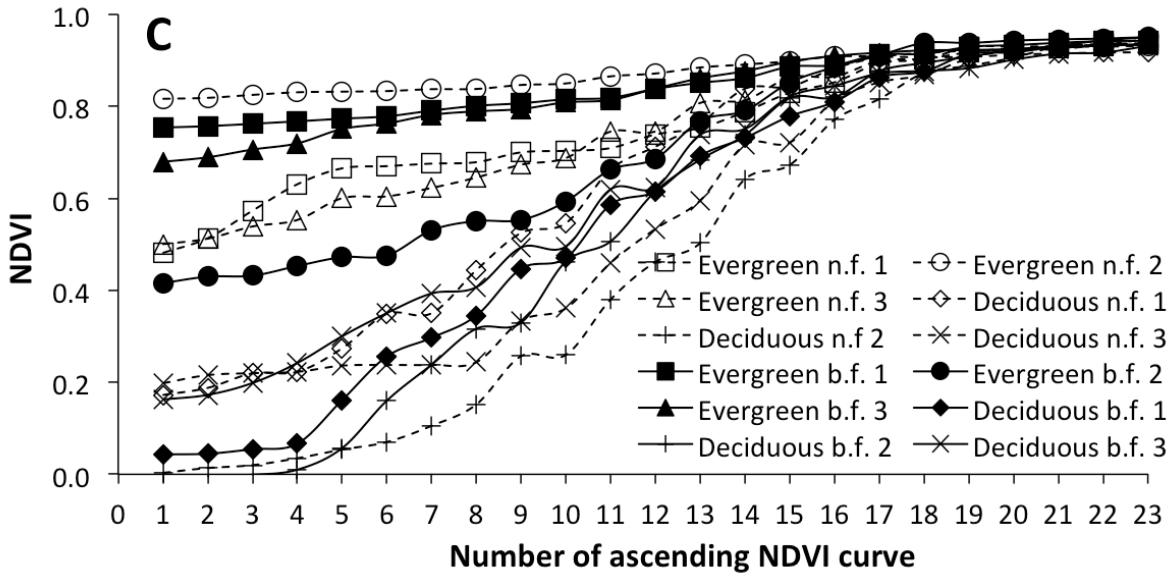

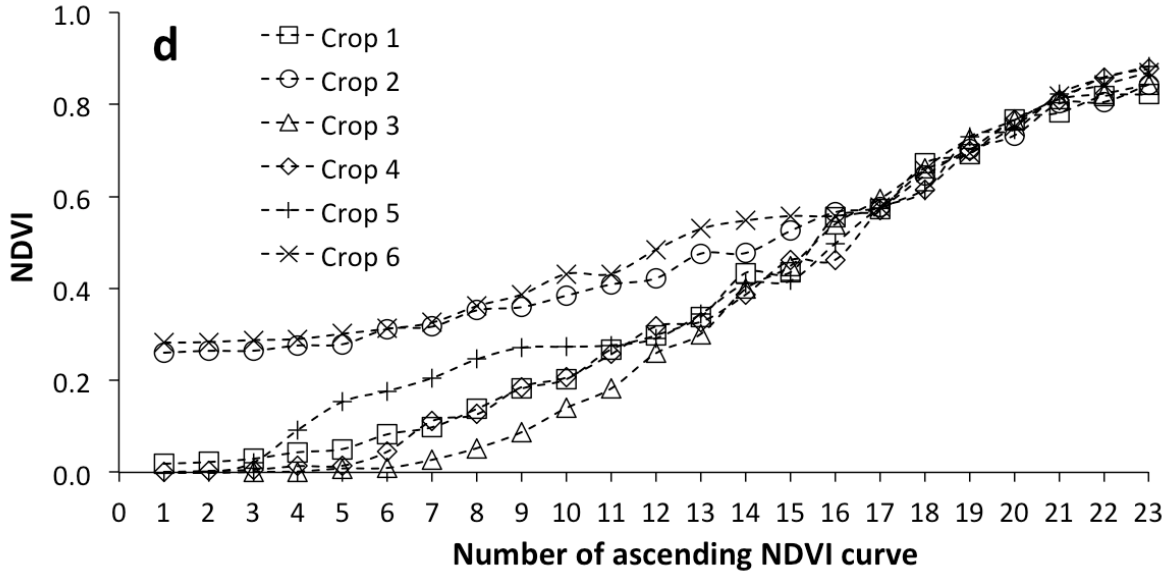

Fig.2 Examples of NDVI temporal profiles of four pure vegetation classes. (a) original NDVI temporal profiles of the four major forests (3 samples, respectively); (b) sorted NDVI temporal profiles of the four major forests; (c) original NDVI temporal profiles of crop fields (6 samples); (d) sorted NDVI temporal profiles of crop fields.

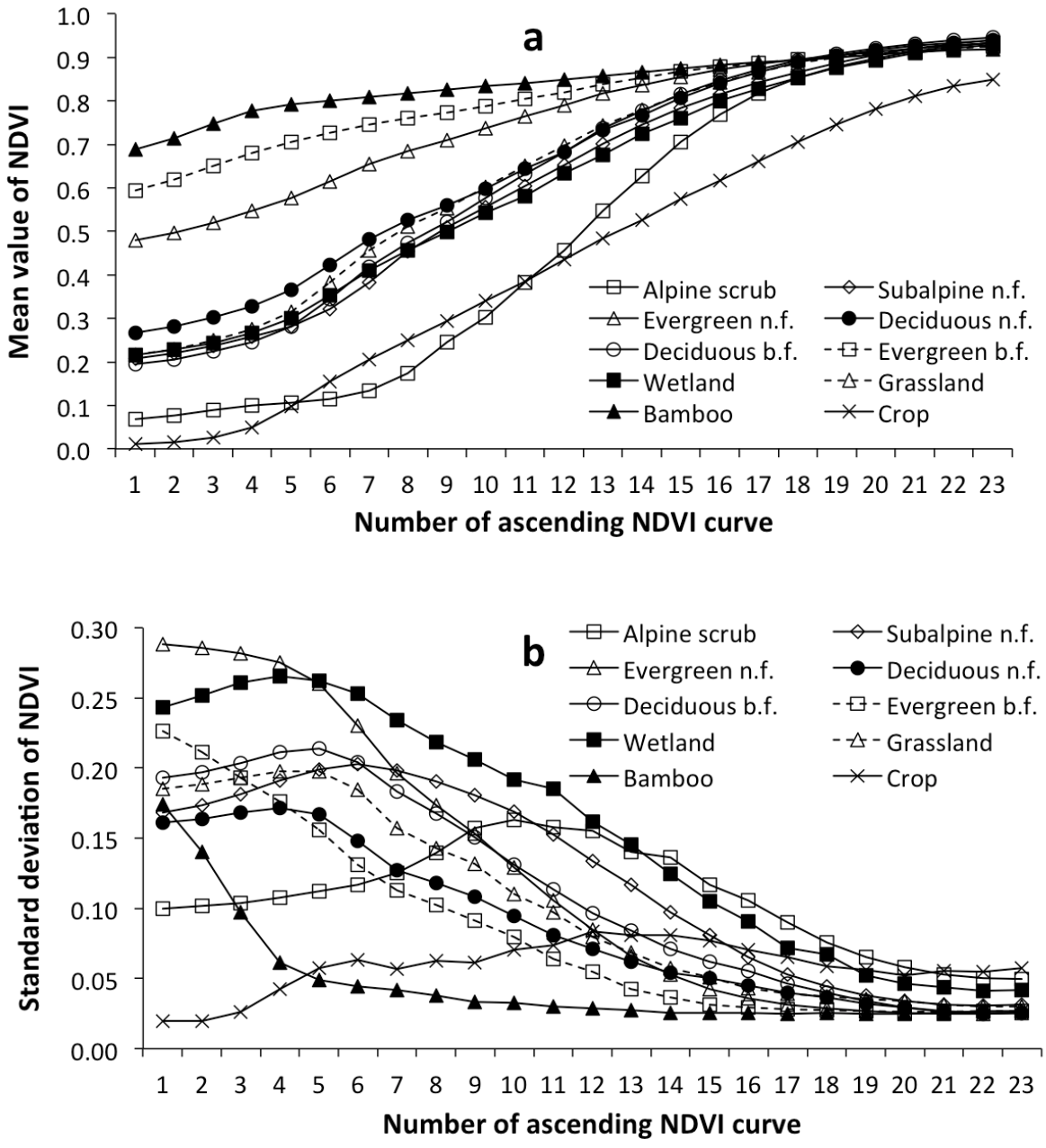

Fig.3 Sorted NDVI temporal profiles and paired standard deviations of pure vegetation. (a) mean NDVI value of pure pixels in each vegetation class after sorting; (b) standard deviation of NDVI in each vegetation class after sorting.

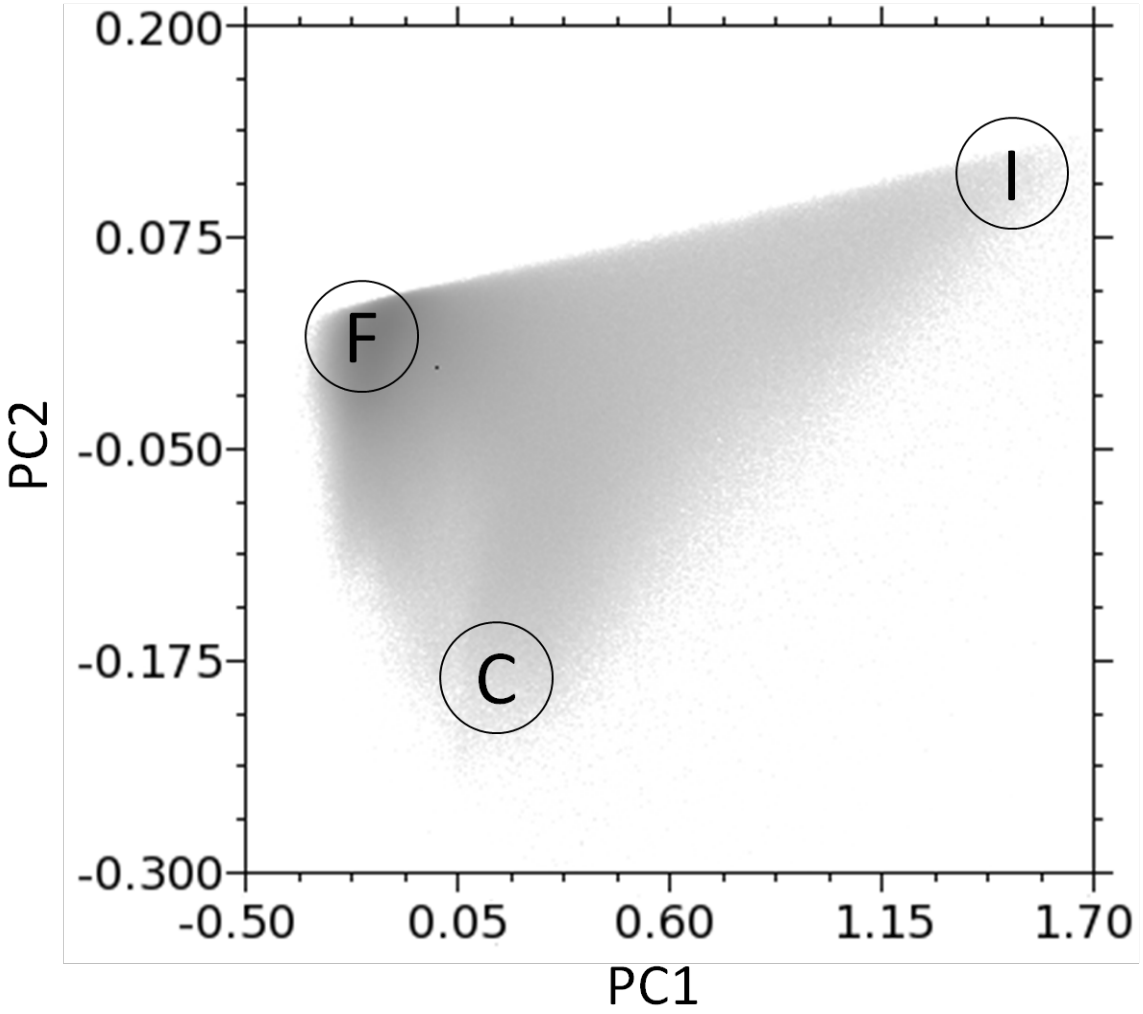

Fig.4 Feature space representation of the first and second principle components transformed from the last six sorted NDVI time-series for temporal mixture analysis. Three endmembers were found. I: impervious surface area; F: forest; C: crop.

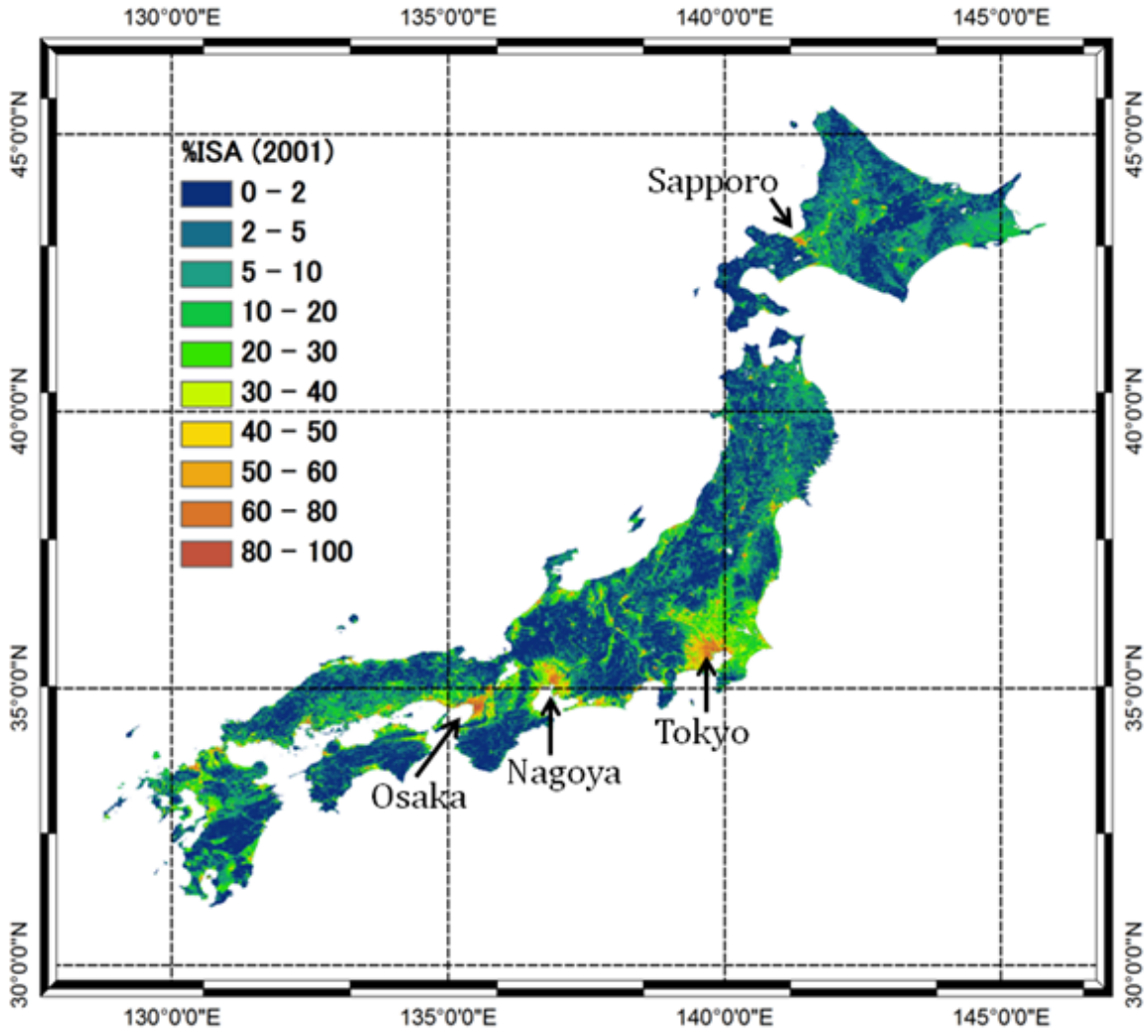

Fig.5 Distribution of impervious surface area estimated by temporal mixture analysis in Japan

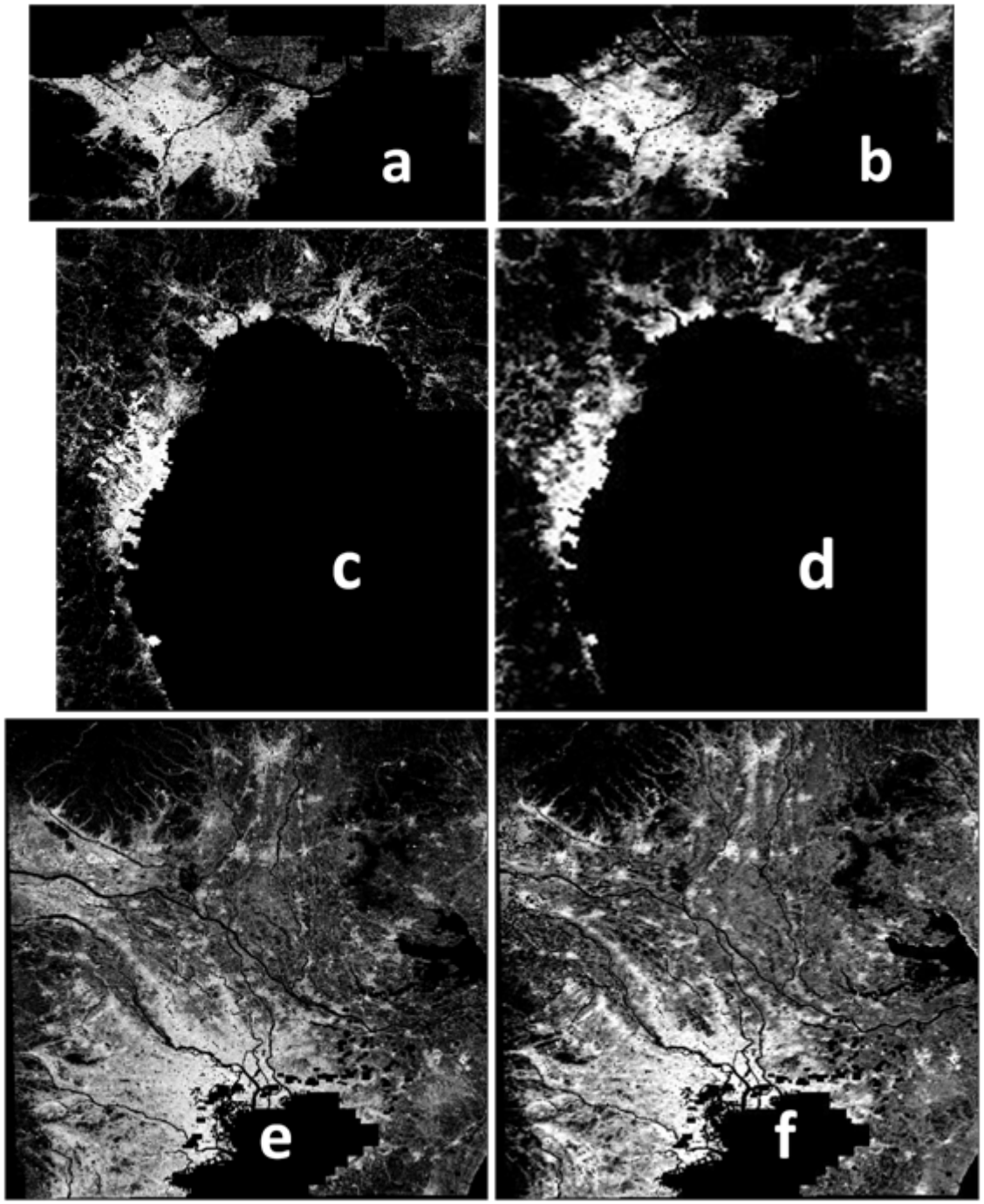

Fig.6 Reference (left, from Landsat-5 TM) and estimated (right, by TMA) impervious surface area map. The reference ISA map has a spatial resolution of 30 m, while the estimated one has a resolution of 250 m. (a) ISA fraction map calculated by pre-screened and normalized multiple endmember SMA (PNMESMA) in Sapporo; (b) ISA fraction map estimated by temporal mixture analysis (TMA) in Sapporo; (c) ISA fraction map calculated by PNMESMA in Kagoshima; (d) ISA fraction map estimated by TMA in Kagoshima; (e) ISA fraction map calculated by PNMESMA in Kanto; (f) ISA fraction map estimated by TMA in Kanto.

1

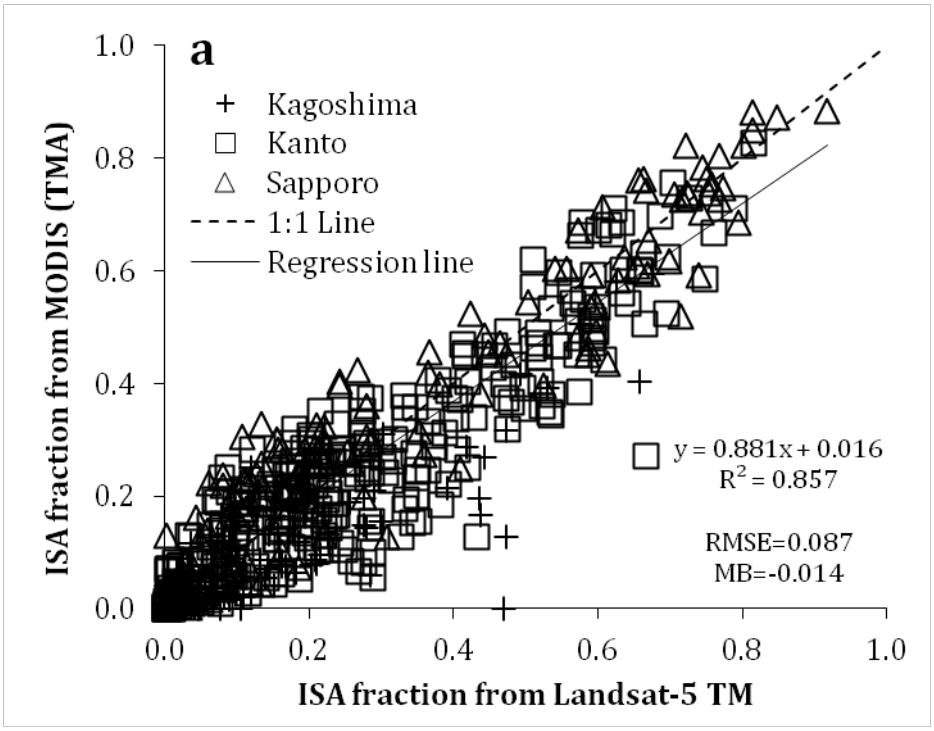
a
Kagoshima
Kanto
Sapporo
1:1 Line
Regression line
y = 0.881x + 0.016
R2 = 0.857
RMSE=0.087
MB=-0.014
ISA fraction from MODIS (TMA)
ISA fraction from Landsat-5 TM
0.0
0.2
0.4
0.6
0.8
1.0

2

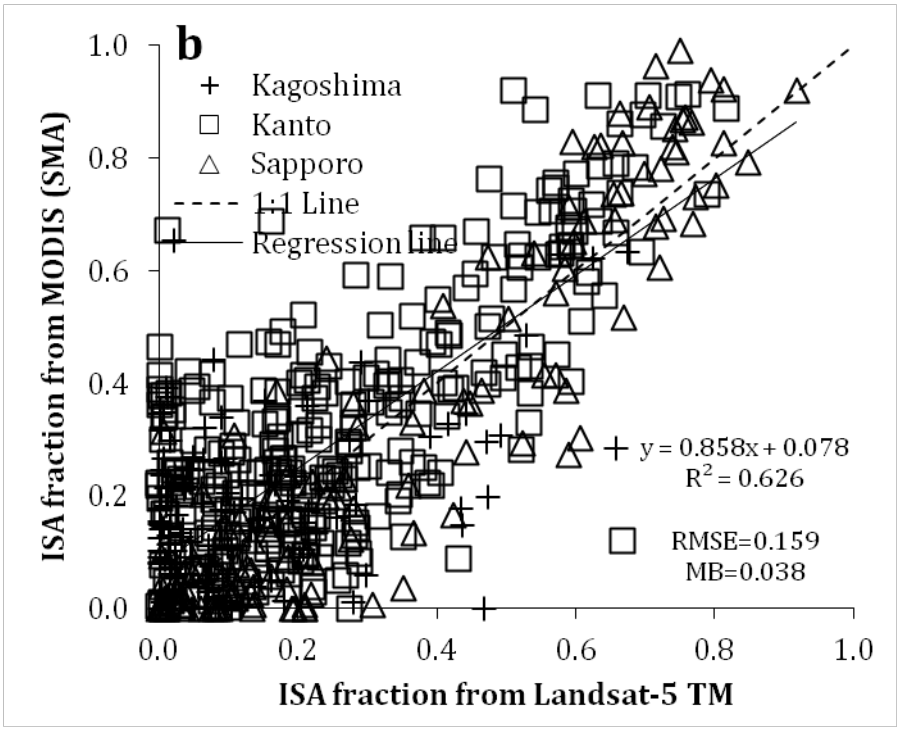
b
Kagoshima
Kanto
Sapporo
1:1 Line
Regression line
y = 0.858x + 0.078
R2 = 0.626
RMSE=0.159
MB=0.038
ISA fraction from MODIS (SMA)
ISA fraction from Landsat-5 TM
0.0
0.2
0.4
0.6
0.8
1.0

3

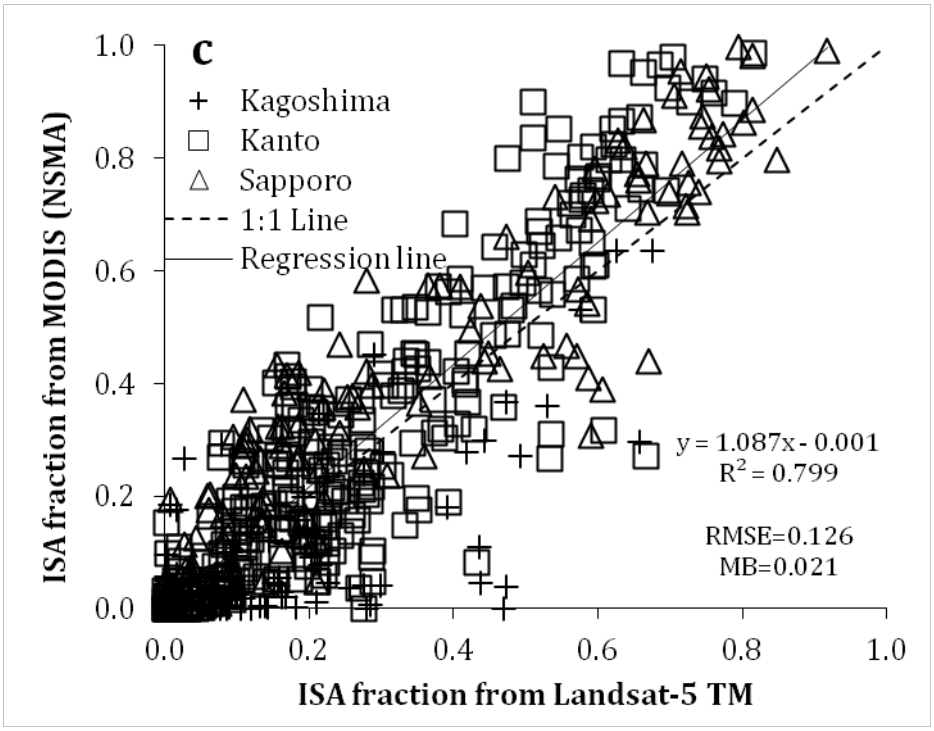

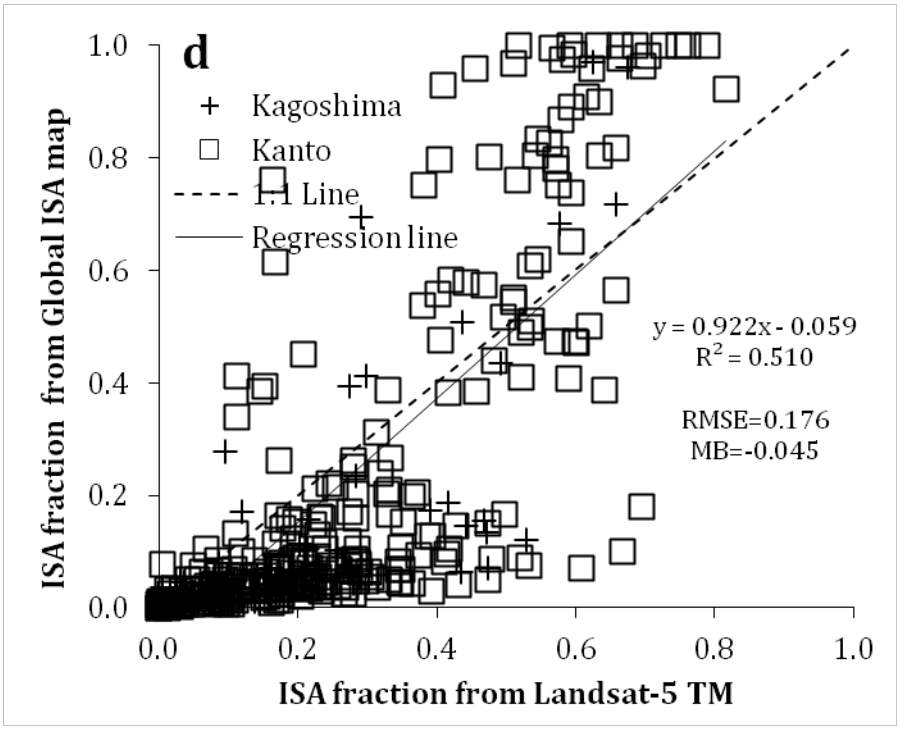

Fig.7 Accuracy assessment of the four methods. (a) TMA: temporal mixture analysis; (b) SMA: spectral mixture analysis; (c) NSMA: normalized SMA; (d) Global: global ISA map